782 *Biochemistry* **2010,** *49,* 782–792
DOI: 10.1021/bi901446r

BIOCHEMISTRY
including biophysical chemistry & molecular biology
Article

Mapping of the Signal Peptide-Binding Domain of *Escherichia coli* SecA Using Förster Resonance Energy Transfer[†]

Sarah M. Auclair,[‡] Julia P. Moses,[§] Monika Musial-Siwek,[§] Debra A. Kendall,[§] Donald B. Oliver,[‡] and Ishita Mukerji*[,‡]

[‡]*Department of Molecular Biology and Biochemistry, Molecular Biophysics Program, Wesleyan University, Middletown, Connecticut 06459 and* [§]*Department of Molecular and Cell Biology, The University of Connecticut, Storrs, Connecticut 06269*

Received August 17, 2009; Revised Manuscript Received December 18, 2009

ABSTRACT: Identification of the signal peptide-binding domain within SecA ATPase is an important goal for understanding the molecular basis of SecA preprotein recognition as well as elucidating the chemo-mechanical cycle of this nanomotor during protein translocation. In this study, Förster resonance energy transfer methodology was employed to map the location of the SecA signal peptide-binding domain using a collection of functional monocysteine SecA mutants and alkaline phosphatase signal peptides labeled with appropriate donor−acceptor fluorophores. Fluorescence anisotropy measurements yielded an equilibrium binding constant of 1.4 or 10.7 μM for the alkaline phosphatase signal peptide labeled at residue 22 or 2, respectively, with SecA, and a binding stoichiometry of one signal peptide bound per SecA monomer. Binding affinity measurements performed with a monomer-biased mutant indicate that the signal peptide binds equally well to SecA monomer or dimer. Distance measurements determined for 13 SecA mutants show that the SecA signal peptide-binding domain encompasses a portion of the preprotein cross-linking domain but also includes regions of nucleotide-binding domain 1 and particularly the helical scaffold domain. The identified region lies at a multidomain interface within the heart of SecA, surrounded by and potentially responsive to domains important for binding nucleotide, mature portions of the preprotein, and the SecYEG channel. Our FRET-mapped binding domain, in contrast to the domain identified by NMR spectroscopy, includes the two-helix finger that has been shown to interact with the preprotein during translocation and lies at the entrance to the protein-conducting channel in the recently determined SecA−SecYEG structure.

Proteins are secreted across or integrated into biological membranes by means of a variety of protein translocation systems that have been characterized over the past several decades. In *Escherichia coli*, the major pathway for protein secretion is the general secretion (Sec) pathway that is composed of two fundamental components: the SecYEG heterotrimeric complex that comprises the protein-conducting channel and the SecA ATPase nanomotor that drives transport of preproteins across the plasma membrane (*1*, *2*). SecA is a 102 kDa multi-domain protein that is present in cytosolic, phospholipid, and SecYEG-bound states (*3*−*5*). In solution, SecA is found in a concentration-dependent equilibrium between monomer and dimer (*6*) that can be shifted by temperature and salt concentration as well as interaction with a variety of translocation ligands such as phospholipids and SecYEG protein (see ref *7* and references cited therein). Whether SecA functions as a monomer or dimer or alternates between these two states during the translocation cycle is currently a matter of controversy (see ref *7* and references cited therein). Once SecA has bound ATP and its preprotein cargo and is properly oriented at the SecYEG channel, ATP hydrolysis is the driving force for SecA-mediated preprotein translocation, which proceeds through a series of conformational changes known as SecA's membrane insertion and retraction cycle (*8*, *9*).

Recently, a model for preprotein translocation has been proposed on the basis of a SecA−SecYEG cocrystal structure (*10*) and disulfide cross-linking studies (*11*). In this model, SecA captures the preprotein in a clamp formed by nucleotide-binding domain 2 (NBD-2)[1], the preprotein binding domain (PPXD), and the helical scaffold domain (HSD) (Figure 1). A two-helix hairpin or "finger" of HSD is proposed to respond to SecA ATPase activity and push the preprotein into the SecY pore. ATP hydrolysis leads to a concerted opening and closing of the clamp as well as an up-and-down movement of the two-helix finger, which drives the translocation of successive segments of the preprotein through the protein-conducting channel. This model implicates specific regions of SecA for preprotein binding and underscores the importance of elucidating the binding interaction under physiological conditions.

[†]This work was supported by Grants GM42033 and GM37639 from the National Institutes of Health to D.B.O. and D.A.K., respectively, and from the Patrick and Catherine Weldon Donaghue Medical Research Foundation (DF#00-118) and the National Science Foundation (MCB-031665) to I.M.

*To whom correspondence should be addressed. Telephone: (860) 685-2422. Fax: (860) 685-2141. E-mail: imukerji@wesleyan.edu.

[1]Abbreviations: CTL, carboxyl-terminal linker domain of SecA; FRET, Förster resonance energy transfer; HPLC, high-performance liquid chromatography; HSD, helical scaffold domain of SecA; HWD, helical wing domain of SecA; IAEDANS, 5-({[(2-iodoacetyl)amino]ethyl}amino)-naphthalene-1-sulfonic acid; IANBD, *N*-{[2-(iodoacetoxy)ethyl]-*N*-methyl}-amino-7-nitrobenz-2-oxa-1,3-diazole; IMV, inverted membrane vesicles; KRR-LamB, λ receptor protein signal peptide with an amino-terminal extension; NBD-1, nucleotide-binding domain 1 of SecA; NBD-2, nucleotide-binding domain 2 of SecA; PPXD, preprotein cross-linking domain of SecA; SP2, alkaline phosphatase signal peptide with a cysteine/IANBD label at position 2; SP16, alkaline phosphatase signal peptide with a cysteine/IANBD label at position 16; SP22, alkaline phosphatase signal peptide with a cysteine/IANBD label at position 22; TKE, 25 mM Tris-HCl (pH 7.5), 25 mM KCl, and 1 mM EDTA buffer.

 Published on Web 12/21/2009

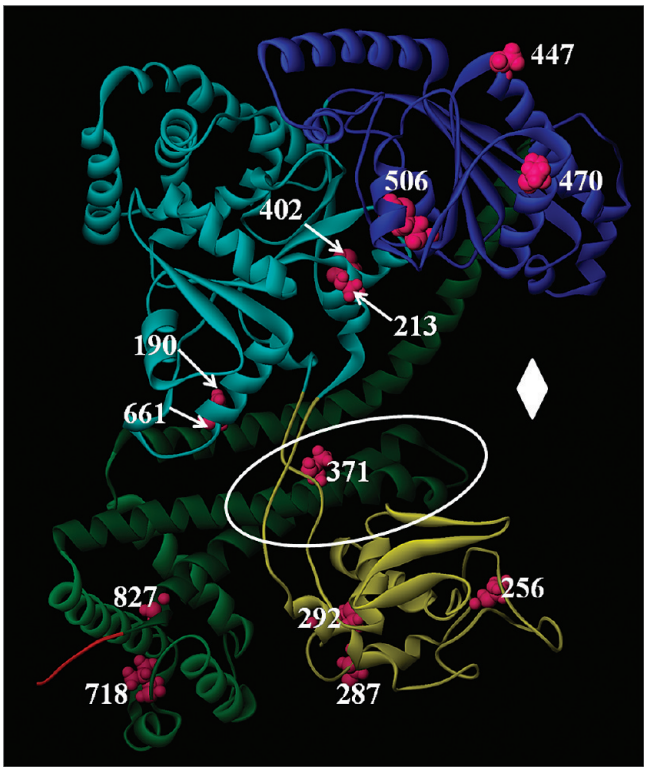

FIGURE 1: Location of SecA domains and cysteine residues. A model of the NMR structure of *E. coli* SecA (Protein Data Bank entry 2VDA structure 1) (*38*) is shown in ribbon representation. The structure of SecA is colored according to domains: light blue for NBD-1, dark blue for NBD-2, yellow for PPXD, dark green for HSD, light green for HWD, and red for the structured portion of CTL. The SecA monocysteine residues used in this study are colored magenta and are labeled with their residue number. The two-helix finger is in the region that falls within the white oval, and the clamp region is identified with a white diamond (*10*).

SecA can acquire its preprotein cargo either by direct interaction with nascent or newly released polypeptide chains or by their transfer from SecB protein, an export-dedicated chaperone that maintains preproteins in their secretion-competent state prior to their engagement with SecA (*12*−*14*). Several lines of evidence indicate that SecA interacts directly with preproteins and, in particular, the signal peptide portion of the preprotein. These include (i) preprotein-dependent stimulation of SecA ATPase activity (termed translocation ATPase activity) and its competitive inhibition by functional signal peptides (*15*, *16*), (ii) inhibition of the ATPase activity of a 64 kDa proteolytic fragment of SecA by functional signal peptides (*17*), (iii) stimulation of SecA ATPase activity in liposomes containing signal peptide alone or in combination with the mature portion of secretory proteins (*18*−*20*), (iv) cross-linking of preproteins or signal peptides to SecA either free in solution, as ribosome-associated nascent chains, or in the presence of liposomes or inverted membrane vesicles (*11*, *14*, *19*, *21*, *22*), and (v) changes in SecA conformation upon signal peptide or preprotein binding (*19*, *20*, *23*−*26*). These studies along with a recent NMR study have also shown that both the positively charged amino-terminal and hydrophobic core regions of the signal peptide are important for SecA binding (*20*, *27*−*29*). Earlier biochemical studies have also demonstrated the critical importance of the hydrophobic core region for signal peptide function where defects in the amino-terminal region are suppressed if the core is of sufficient length and hydrophobicity (*28*, *30*). Insertion of polar or charged amino acid residues within this region also results in secretion defects, further demonstrating the importance of the hydrophobic core region for signal peptide function (*31*−*33*).

A number of approaches have been utilized to define the signal peptide or preprotein-binding region of SecA. Many of them have utilized genetically truncated SecA proteins along with binding or cross-linking assays using preproteins or signal peptides to map the relevant ligand-binding site. Originally, chemical cross-linking of a preprotein to an overlapping family of truncated SecA proteins allowed localization of a preprotein-binding region to residues 267−340 of SecA, which comprises most of the PPXD domain (*21*). The weakly structured, globular PPXD domain is formed by *E. coli* SecA residues 221−377 and is connected to NBD-1 by residues 222−229 and 369−376, which form β-strands in the *Bacillus subtilis* SecA structure and are unstructured in the recently determined *E. coli* SecA structure (see Figure 1) (*3*, *34*). More precise deletion mutagenesis of SecA narrowed the signal peptide and mature region-binding domains to residues 219−244 and 221−377, respectively (*25*, *35*). An alternative approach to this problem utilized a signal peptide containing a photoaffinity label and a family of full-length SecA proteins with engineered Factor Xa cleavage sites to identify a signal photolabeled region within residues 269−322 of SecA (*36*). Genetic analysis of the PPXD domain of SecA identified Leu-319 as a critical residue in facilitating SecA signal peptide binding, while Tyr-326 was shown to be important for the SecA preprotein binding and release cycle (*26*, *37*). Studies of disulfide cross-linking of a nascent preprotein to SecA point to an interaction between the tip of the two-helix finger of HSD and the preprotein; specifically, SecA residues 795, 797, and 798 were observed to cross-link strongly to the polypeptide chain (see Figure 1). In addition, an important role for Tyr-794 was implicated in these studies, where mutation of this position with anything but a bulky hydrophobic residue weakened the interaction between SecA and the preprotein (*11*). Recently, more structural biological approaches have been taken to refine this picture. A solution NMR structure of SecA bound to an artificially extended amino-terminal signal peptide, KRR-LamB, has been presented. In this case, the signal peptide-binding domain is largely contributed by residues within PPXD with a smaller contribution from HSD, and the orientation of the bound signal peptide is essentially parallel to the PPXD "connector" strands and orthogonal to the helices of the two-helix finger subdomain of SecA (*38*). In a second study, site-directed spin labeling and electron paramagnetic resonance spectroscopy were utilized to identify the region of SecA that binds to two different preproteins. A single interactive surface comprised of the SecA amino terminus along with the NBD-2, PPXD, and HSD domains was identified, which largely corresponded to the groove containing SecA's preprotein clamp proposed by Zimmer et al. (*10*, *39*). Further support of the identification of this area for peptide binding is found in a recent cocrystal structure of SecA in which electron density for bound peptide is detected at the back of this clamp area (*40*). Thus, all of these studies are consistent with the importance of the PPXD domain of SecA for signal sequence and preprotein binding, and the more recent studies indicate the importance of the HSD and perhaps certain interfacial portions of NBD-1, NBD-2, and HWD for ligand binding.

While the aforementioned studies have narrowed this problem considerably, some uncertainty still surrounds the precise location of the SecA signal peptide-binding domain (particularly at

the atomic level) given a variety of technical limitations with each of these approaches. Many genetic or biochemical approaches are limited since they essentially utilize linear mapping techniques or probe a small number of amino acid residues to localize a three-dimensional ligand-binding domain. Any regions identified by such approaches may be peripheral to the actual ligand-binding site or include only a portion of it. Furthermore, chemical or photochemical preferences in cross-linking or conformational or other sorts of defects in truncated or mutant SecA proteins could bias or compromise such data sets. Since most of these techniques lack atomic resolution, they are generally unable to delineate the precise peptide-binding motifs on SecA. Finally, while structural approaches to this problem possess the requisite resolution, certain approaches (e.g., X-ray crystallography and NMR spectroscopy) require extraordinarily high protein and peptide concentrations that could promote nonphysiological ligand binding, while other approaches (e.g., electron paramagnetic resonance spectroscopy) are sensitive to changes in protein conformation that can mask or mimic ligand binding.

FRET methodologies have been widely applied to measuring intersite distances in macromolecules with well-placed fluorophores. Recently, single-molecule FRET techniques in addition to equilibrium FRET measurements have led to an improved understanding of dynamic cellular mechanisms, formation of macromolecular complexes, protein−DNA interactions, mapping of ligand-binding sites on proteins, and examination of conformational changes within proteins (*41*−*43*). Three-dimensional information from FRET-based measurements has been obtained by the engineering of probe location with the use of site-directed mutagenesis in relevant target areas (see refs *44* and *45* and references cited therein for examples). Although the relative motion of the probes and the extent of energy transfer can limit the accuracy of distance measurements, with appropriate probe selection such measurements can approach atomic dimensions. Considerable detail can be obtained on binding sites and conformational changes within proteins whose X-ray or NMR structures are available.

Previous fluorescence studies of SecA have utilized intrinsic tryptophan fluorescence along with collisional quenchers to study SecA conformational changes mediated by binding of signal peptides, nucleotides, model membranes, or SecYEG-containing proteoliposomes (*24*, *46*). FRET has been utilized successfully to study SecA PPXD and HSD interdomain interactions that are modulated by nucleotide and lipid binding (*47*), as well as to assess the dimeric form of SecA in solution and to study its stability in the presence of phospholipids, signal peptides, and nucleotides (*48*, *49*).

In this study, we have developed a FRET methodology for mapping the location of the bound signal peptide on SecA. These studies were conducted using a collection of functional monocysteine SecA mutants labeled with a donor fluorophore and alkaline phosphatase signal peptides labeled with an acceptor fluorophore to give unique and appropriate distance information. By using the FRET technique, which employed a native signal peptide at more biochemically relevant SecA protein concentrations, we were able to work under conditions where concerns about nonphysiological ligand binding were minimized. Such conditions are particularly important given the hydrophobic nature of both the signal peptide and SecA protein. Our results place the signal peptide-binding domain near the center of the SecA protomer where it is flanked by domains critical for the binding of nucleotide, the remainder of the preprotein, and SecYEG. The domain identified here overlaps with the functionally equivalent region delineated in the NMR structure of the SecA−signal peptide complex (*38*). However, our study shows a more extensive contribution of the HSD domain to the binding site, and it suggests a model in which signal peptide binding may occur in parallel rather than orthogonal to HSD by more extensive interaction with the HSD α-helices. This latter suggestion is consistent with recent biochemical cross-linking and structural studies that implicated the two-helix finger of HSD acting as a ratchet to drive preprotein translocation through the SecYEG channel (*10*, *11*). The importance of the HSD domain of SecA in preprotein interaction was also observed in the recent EPR-based mapping study (*39*).

EXPERIMENTAL PROCEDURES

Materials. SP-Sepharose, hexyl agarose, β-mercaptoethanol, spectroscopic grade Tris-HCl, and most other reagent quality chemicals were from Sigma. The fluorescent probes, IAEDANS and IANBD-Ester, were obtained from Invitrogen. The *E. coli* alkaline phosphatase signal peptide SP22, MKQSTIALALL-PLLFTPVTKAC-NH_2, SP2, MCKQSTIALALLPLLFTPVT-KA-NH_2, and scrambled modified SP22, PLMDTEITLKF-LSPLQALKTVC-NH_2, were synthesized by Biomolecules Midwest Inc. The cysteine residues incorporated into the peptides provided the target for IANBD labeling, while the carboxyl terminus of the peptides was capped with an amide to prevent an unnatural negative charge (*20*). Peptides were purified via HPLC, and their identity was verified with electrospray ionization mass spectrometry at the Keck Biotechnology Resource Laboratory at Yale University (New Haven, CT).

Monocysteine SecA Mutant Protein Expression and Purification. *E. coli* BL21.19 [*secA13*(*Am*) *supF*(*Ts*) *trp*(*Am*) *zch*::*Tn10 recA*::*CAT clpA*::*KAN*] is derived from BL21-(λDE3) (*50*) and was used as the host for all *secA*-containing plasmids. Plasmid pT7secA-Cys-0, a derivative of pT7secA2 that has all four cysteine codons within *secA* changed to serine, and its monocysteine-encoding derivatives have been described previously (*51*). pT7secAΔ11-Cys-190 was constructed from pT7secA-Cys-190 using primers (Integrated DNA Technologies) designed to remove nucleotides corresponding to residues 2−11 using the site-directed QuikChange mutagenesis kit as described by the manufacturer (Stratagene). All *secA* mutants were verified by DNA sequence analysis at the University of Pennsylvania DNA sequence facility. The plasmids were transformed into BL21.19 cells and checked for *secA* complementation by comparing their plating efficiency at 42 and 30 °C as described previously (*52*).

Most SecA monocysteine mutant proteins were overproduced and purified as described previously (*48*) with the following modification: the biomass was washed with 10 mM Tris-HCl (pH 7.5), 50 mM KCl, and 10 mM MgOAc and dialyzed against 25 mM Tris-HCl (pH 7.5), 25 mM KCl, 0.5 mM EDTA, and 0.5 mM phenylmethanesulfonyl fluoride. His-tagged SecA protein was purified utilizing a HisBind resin column (Novagen) according to the manufacturer's protocol. The protein concentration was determined using the Bradford assay (Bio-Rad) with bovine serum albumin as the standard.

Signal Peptide Labeling. The signal peptide was dissolved in dimethyl sulfoxide to a concentration of 3 mM, and IANBD was dissolved in dimethyl sulfoxide to a final concentration of 10 mM. Signal peptide was diluted into 10 mM phosphate buffer (pH 7) to a final concentration of 200 μM, and IANBD was added to the

reaction mixture in a dropwise fashion to a final concentration of 2 mM. The reaction mixture was incubated at room temperature for 4 h with shaking, and the reaction was terminated when the mixture was frozen at −80 °C. The labeled signal peptide was purified by HPLC on a Vydac Silica Gel 214 TP-1010 column and then lyophilized. It was then dissolved in dimethyl sulfoxide at a final concentration of 3 mM and stored at −80 °C until it was used. The degree of labeling was calculated according to the manufacturer's instructions (Molecular Probes) and was approximately 100%. Labeling efficiency was confirmed by electrospray ionization mass spectrometry at the Keck Biotechnology Resource Laboratory at Yale University, where the level of unlabeled peptide was undetectable in the mass spectrum of the labeled peptide sample.

SecA Monocysteine Mutant Labeling. Monocysteine SecA mutant proteins at a concentration of 10 μM in TKE [25 mM Tris-HCl (pH 7.5), 25 mM KCl, and 1 mM EDTA] were labeled with IAEDANS at a 20-fold molar excess for 4 h at room temperature. The samples were quenched with 1 mM β-mercaptoethanol for 30 min. Free IAEDANS was removed from the sample by repeated addition of TKE and sedimentation through a Centriprep concentrator (Millipore) until the absorbance at 336 nm of the eluate was zero and its fluorescence spectrum was similar to that of the buffer. Labeled SecA proteins were stored in TKE supplemented with 20% glycerol at −80 °C until use.

SecA ATPase Activity. SecA ATPase activities were determined by the Malachite green method (*53*) utilizing the modifications described previously (*54*). ATPase activity was calculated using the following formulas: endogenous ATPase activity = ATPase activity in the presence of SecA − ATPase activity in the absence of SecA; membrane ATPase activity = ATPase activity in the presence of SecA and IMV − endogenous ATPase activity; translocation ATPase activity = ATPase activity in the presence of SecA, IMV, and preprotein − membrane ATPase activity.

Fluorescence Measurements. Fluorescence anisotropy and intensity spectra were recorded on a FluoroMax-2 spectrofluorometer (Horiba Jobin Yvon) with a programmable water bath (RTE model 111, NESLAB Instruments, Inc.). The samples were placed in a quartz cuvette (Starna Cell, Inc.) with a 3 mm path length. The spectral bandwidths of the excitation and emission slits were set at 4 and 6 nm, respectively. The integration time for the intensity measurement was typically 0.5 s/data point. Final values result from at least three separate experiments of at least three scans for each sample.

Anisotropy experiments were conducted with samples containing 1 μM IANBD-labeled alkaline phosphatase signal peptide in TKE buffer. SecA was added to the samples over a concentration range from 0 to 40 μM and incubated for 30 min before data collection. Samples were excited at 480 nm and measured at 550 nm. Data were fit assuming a 1:1 binding interaction (vide infra) using Origin version 6.0 with the following equation:

$$y = A_0 + (A_i - A_0)\left(\frac{[SP] + K_d + [P] - 4[SP][P]}{2[P]}\right) \quad (1)$$

where [SP] is the total concentration of the signal peptide, [P] is the total concentration of SecA protein, K_d is the equilibrium dissociation constant, A_0 is the anisotropy of the signal peptide in the absence of SecA, and A_i is the anisotropy under saturating binding conditions.

For fluorescence intensity spectra, unlabeled or IAEDANS-labeled SecA (7 μM) and unlabeled or IANBD-labeled alkaline phosphatase signal peptide (18 μM) were incubated together in various combinations in TKE buffer for 30 min at room temperature. The polarizers were set at the magic angle (0° and 55°), and the samples were scanned at a rate of 1 nm/s at 20 °C. Samples were excited at 336 nm and measured from 346 to 660 nm.

The equilibrium binding constant of SecAΔ11-Cys-190 was measured using a FRET titration, where protein was maintained at 0.05 μM and IANBD-labeled SP22 was titrated over a range of 0−20 μM. Energy transfer was calculated for each signal peptide concentration, and those values were plotted using Origin version 6.0 and fitted with eq 1.

FRET Calculation. All spectra were corrected for the background. Donor or acceptor only spectra were collected in the presence of the unlabeled counterpart to correct for any changes in fluorescence intensity as a consequence of binding. SP2 FRET data were corrected for the percent of signal peptide bound in the experiment (53%). SP22 FRET data were collected at saturation, and no correction for percent bound was needed.

The FRET efficiency, E, was calculated on the basis of the quenching of the donor fluorescence intensity in the FRET complex relative to the donor only emission in the presence of unlabeled peptide. The efficiency of energy transfer is calculated using the following equation (*55*):

$$E = 1 - (F_{DA} - F_A)/F_D \quad (2)$$

where F_{DA}, F_D, and F_A are the fluorescence intensities of the FRET pair, donor alone, and acceptor alone, respectively. The donor alone spectra were collected in the presence of unlabeled signal peptide to correct for any changes in fluorescence induced by peptide binding. Similarly, acceptor only spectra were collected in the presence of unlabeled SecA to account for any changes induced by binding. Although the efficiency was calculated from the decrease in donor emission, the observation of FRET was confirmed by the appearance of enhanced acceptor emission (Figure S1 of the Supporting Information). The donor decrease was determined to be more reliable and consistent because of trace amounts of free acceptor dye. The efficiency of energy transfer is related to R_0, the Förster distance, and R, the distance between donor and acceptor, by the equation

$$E = R_0^6/(R_0^6 + R^6) \quad (3)$$

R_0 is defined as the distance at which the transfer is 50% efficient and is calculated (in angstroms) as follows (*55*):

$$R_0 = 0.211[n^{-4}Q_D\kappa^2 J(\lambda)]^{1/6} \quad (4)$$

In eq 4, n is the refractive index [assumed to be 1.4 for biomolecules in aqueous solution (*55*)], κ is the orientation factor (κ^2 was assumed to be $^2/_3$ for a randomly oriented, mobile donor and acceptor pair), and Q_D is the quantum yield of the donor in the absence of acceptor. $J(\lambda)$, the overlap integral between donor emission and acceptor absorption, is calculated from the spectral data by (*55*)

$$J(\lambda) = \int [\varepsilon_A(\lambda)\lambda^4] f_D(\lambda)\, d\lambda \quad (5)$$

where $\varepsilon_A(\lambda)$ is the molar extinction coefficient for the acceptor (M^{-1} cm^{-1}) and f_D is the fluorescence intensity of the donor at wavelength λ (nanometers).

The quantum yield of IAEDANS-labeled SecA in the absence of acceptor was measured relative to quinine sulfate (Φ = 0.56) (*56*). Quantum yields for IAEDANS-labeled SecA-Cys-190, SecA-Cys-661, and SecA-Cys-827 could not be accurately determined; therefore, the average R_0 value of 33.7 Å (see Table 1) was used to calculate distances for those cases as well as for the SecA-Cys-256/SP2 pair.

RESULTS AND DISCUSSION

Experimental Design and Functional Activity of Dye-Labeled SecA Mutants. We have developed a FRET-based SecA signal peptide binding assay as an alternative structural method for mapping the SecA signal peptide-binding domain at more standard biochemical protein concentrations. To this end, we employed SecA proteins purified from our collection of functional monocysteine *secA* mutants (Figure 1) (*51*) and two alkaline phosphatase signal peptides with cysteine incorporated at residue 2 (SP2) or 22 (SP22). These cysteine residues allowed us to specifically incorporate appropriate donor and acceptor dyes into our system by sulfhydryl chemistry. The addition of a C-terminal cysteine residue onto the alkaline phosphatase signal peptide did not affect translocation or cleavage kinetics in vivo (*57*), while amino acid additions or substitutions within the amino-terminal region of the signal peptide should be functionally tolerated as long as the hydrophobic core region contains sufficient hydrophobicity (*28*, *30*).

We chose to utilize the IAEDANS−IANBD pair since these two dyes have been used successfully in previous FRET studies (for examples, see refs *58* and *59*). The relatively short R_0 value [34 Å measured for the free dyes (data not shown)] was considered appropriate for the resolution needed to map the binding site on a large protein like SecA [~100 Å in its longest dimension (*34*)]. In addition, SP22 labeled with one of these dyes was previously shown to bind to SecA with an affinity comparable to that of control signal peptides under physiological conditions (*26*).

IAEDANS-labeled SecA proteins were tested for their ATPase activities to ensure their continued functionality after dye attachment. SecA protein possesses three types of ATPase activity: an endogenous ATPase activity in solution that is stimulated by binding to IMV (membrane ATPase) or IMV and preprotein (translocation ATPase) (*60*). We found that the ATPase activities of the dye-labeled (Figure 2) and unlabeled (data not shown) SecA proteins were similar to that of wild-type SecA, although certain SecA proteins had higher endogenous or membrane ATPase activity (particularly IAEDANS-labeled SecA-Cys-190, SecA-Cys-213, SecA-Cys-661, and SecA-Cys-827 or SecA-Cys-292, SecA-Cys-661, and SecA-Cys-827, respectively), while others displayed modestly reduced translocation ATPase activity (IAEDANS-labeled SecA-Cys-256, SecA-Cys-287, SecA-Cys-718, and SecA-Cys-827). However, previous studies have shown that all mutant SecA proteins that possess ≥30% translocation ATPase activity are active for both in vivo and in vitro protein translocation (D. Oliver, unpublished results). On the basis of these results as well as the in vivo functionality of these SecA proteins, we concluded that our IAEDANS-labeled SecA proteins were active for SecA function.

Signal Peptide Binding Affinity Measured by Fluorescence Anisotropy. Next, SecA binding affinity and stoichiometry for signal peptide were characterized by fluorescence anisotropy. Binding affinity was measured by reverse titration in which increasing concentrations of unlabeled SecA were added to 1 μM IANBD-labeled signal peptide to avoid aggregation of the signal peptide at high concentrations. In addition, the relative change in anisotropy is larger for the signal peptide and therefore yields a greater signal. Since wild-type SecA exhibits a nanomolar monomer−dimer dissociation constant under similar conditions (*6*, *61*), we assume that the SecA was mainly in the dimer form at the concentrations used in this experiment. Although SecA is also hydrophobic in nature, measurements were limited to concentrations at which aggregation was not detected. The large increase in anisotropy of the IANBD-labeled signal peptides was saturable and SecA concentration-dependent, yielding K_d values of 1.4 ± 0.2 and 10.7 ± 3.1 μM for SP22 and SP2,

Table 1: FRET Data for SecA Signal Peptide Binding

	Cys mutant	E_{FRET}[a]	R (Å)[b]	R_0 (Å)[c]
SP22 data	190	0.70	29.2 ± 0.5	33.7
	213	0.21	42.3 ± 0.2	32.4
	256	0.53	26.1 ± 0.2	26.7
	287	0.70	26.2 ± 0.2	30.3
	292	0.33	30.8 ± 1.1	27.5
	371	0.35	37.8 ± 0.5	30.6
	402[d]	0.08	58.3 ± 2.1	39.5
	447[d]	0.15	52.8 ± 1.8	39.5
	470[d]	0.16	51.8 ± 1.9	39.5
	506	0.10	49.1 ± 1.2	34.0
	661	0.53	33.9 ± 3.9	33.7
	718	0.36	37.3 ± 0.1	40.6
	827	0.21	42.4 ± 0.2	33.7
SP2 data	190	0.59	32.1 ± 0.7	33.7
	213	0.66	30.5 ± 0.2	32.4
	256	0.53	39.4 ± 0.3	33.7
	292	0.63	31.1 ± 0.2	27.5
	827	0.50	33.9 ± 0.1	33.7

[a]FRET efficiency (E_{FRET}) was measured by the quenching of the donor fluorescence intensity as described in Experimental Procedures. [b]The donor−acceptor distance (R) was calculated as described in Experimental Procedures. [c]The Förster energy transfer distance defined as 50% efficient. [d]The FRET fluorescent dye pair used included Alexa Fluor-488 and Alexa Fluor-555.

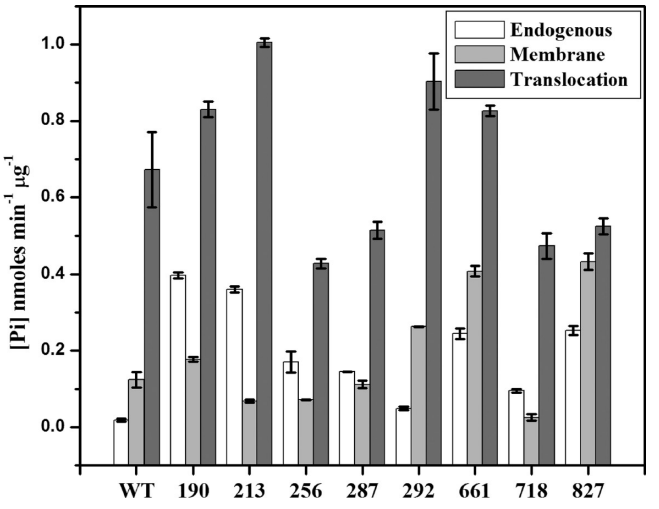

FIGURE 2: ATPase activities of IAEDANS-labeled SecA proteins. The endogenous, membrane, and translocation ATPase activities of the purified monocysteine SecA mutant proteins were determined at 37 °C as described in Experimental Procedures. The data represent an average of at least three different experiments. WT indicates wild-type SecA, while the number indicates the position of the IAEDANS-labeled monocysteine substitution within SecA.

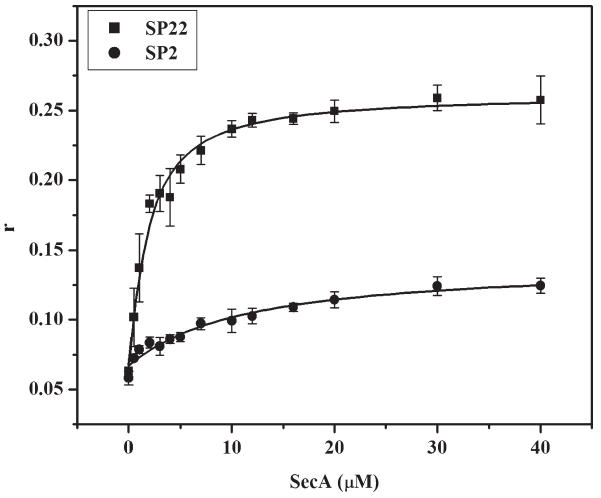

FIGURE 3: Equilibrium binding of the alkaline phosphatase signal peptide to SecA as determined by fluorescence anisotropy. Binding of IANBD-labeled SP22 (■) or SP2 (●) to SecA was assessed by fluorescence anisotropy (r). Signal peptides were maintained at a constant concentration of 1 μM, and wild-type SecA was titrated into the system from 0 to 40 μM. All experiments were performed in TKE buffer at 20 °C.

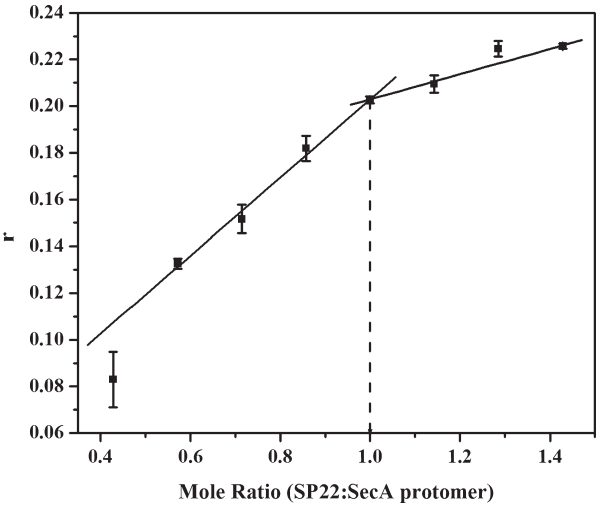

FIGURE 4: Stoichiometry of SecA−signal peptide binding as determined by fluorescence anisotropy. Binding of IANBD-labeled SP22 (■) to SecA was assessed as fluorescence anisotropy (r) and plotted to reveal the saturated molar ratio of SP22 to SecA protomer. IANBD-labeled SP22 was titrated from 0 to 20 μM into a solution of 14 μM wild-type SecA. All experiments were performed in TKE buffer at 20 °C.

respectively (Figure 3). The binding affinity measured for the SP22 peptide is in good agreement with peptide−SecA K_d values previously determined by other methods. Specifically, Kendall and co-workers conducted SP22−IAEDANS competition experiments over a concentration range of the unlabeled signal peptide yielding a K_i of 2.5 ± 0.5 μM (*26*). Also, the K_d value reported here is comparable to the value obtained for SecA and the model signal peptide, 3K7L, using a biosensor approach (*25*) and the EC_{50} for wild-type and model signal peptide-induced stimulation of SecA ATPase activity observed for both the wild-type and model signal peptide (*20*). The weakened affinity observed for the SP2 peptide illustrates the importance of an intact amino-terminal region of the signal peptide for high-affinity interaction with SecA (*26*, *27*). In separate fluorescence binding experiments performed with labeled SecA protein and unlabeled SP2, we were able to establish that the reduced affinity of SP2 results mainly from the presence of the label (Figure S2 of the Supporting Information). When an alkaline phosphatase signal peptide labeled at position 16, SP16, was tested in our binding assay, we were unable to detect specific binding at the concentrations of SecA and signal peptide utilized (data not shown). This latter result agrees with a similar observation that attachment of a nitroxide spin-label to the hydrophobic core region of the KRR-LamB signal peptide inhibited its binding to SecA (*38*), and it underscores the importance of this region for proper SecA−signal peptide interaction.

Stoichiometry of the SecA−Signal Peptide Interaction. The stoichiometry of binding of SP22 to SecA was measured by titration of IANBD-labeled SP22 into a solution of SecA at a concentration of 14 μM, 10-fold greater than the K_d. At this concentration, all of the added signal peptide binds to SecA, as shown by a linear increase in fluorescence anisotropy. Once all the binding sites are filled, a plateau in anisotropy is observed, and the point of discontinuity corresponds to the binding stoichiometry. The plateau in anisotropy occurred at a mole ratio of signal peptide to SecA of 1:1 (Figure 4), a stoichiometry in agreement with previous results (*38*). At higher ratios of signal peptide to SecA, a slight increase in anisotropy was detected, reflecting a nonspecific binding interaction. Since signal peptides tend to aggregate at concentrations above 30 μM, the stoichiometry of binding of SP2 to SecA could not be determined given the high concentrations of SP2 needed to perform this measurement.

Binding Affinity of Signal Peptide for the SecA Monomer or Dimer. To elucidate whether the signal peptide binds preferentially to the SecA monomer or dimer, we measured SecA binding affinity with a monomer-biased mutant lacking N-terminal residues 2−11, SecAΔ11. This SecA mutant has a micromolar monomer−dimer association constant compared to the nanomolar association constant of wild-type SecA at the salt concentrations utilized in our assay system (*6*, *61*). To measure the binding affinity at concentrations where SecAΔ11 is primarily monomeric (≤50 nM), we developed a FRET-based binding assay to give us the necessary sensitivity at these relatively low protein concentrations. For these measurements, we utilized IAEDANS-labeled SecAΔ11Cys-190, since the label at this position results in a relatively high FRET efficiency with the SP22 peptide [E_{FRET} = 0.7 (Table 1)]. Forward titrations in which SecA concentrations were kept constant and signal peptide concentrations were varied were performed. The experiment was performed at a SecA concentration of 50 nM where wild-type SecA is a dimer while SecAΔ11Cys-190 is a monomer [K_d < 1 nM, and K_d = 230 ± 20 nM, respectively, at 25 mM KCl (data not shown); also see refs *6* and *61*]. The SP22 binding curve determined for SecAΔ11Cys-190 yielded essentially the same binding constant as wild-type SecA (3.06 ± 1.13 and 1.4 ± 0.2 μM, respectively). These results suggest that the signal peptide can bind to either SecA monomer or dimer with approximately comparable affinity. While two previous studies indicated that high concentrations of signal peptide can induce SecA monomerization, this effect occurred at a signal peptide concentration higher (≥20 μM) than that utilized here, and furthermore, it has not been observed in all cases (*26*, *49*, *62*). In the cell, the concentration of SecA is estimated to be 5 μM (*49*), but the effect of SecA ligands on the monomer−dimer equilibrium complicates the interpretation of whether translocation occurs

via a SecA monomer, a SecA dimer, or some other type of monomer−dimer association−dissociation cycle (reviewed in ref *7*).

FRET Transfer Efficiencies and Distances. The location of the signal peptide-binding domain of SecA was determined by measuring the distance from each IAEDANS-labeled monocysteine SecA mutant to the bound IANBD-labeled alkaline phosphatase signal peptide using FRET and then determining the intersection of the combined data set. A control study was performed to ensure that removal of the four naturally occurring cysteine residues within SecA and introduction of a mutant cysteine residue did not affect binding affinity for the signal peptide. Fluorescence anisotropy was used to measure the affinity of SecA-Cys-256 for IANBD-labeled SP22 by reverse titration as described above. The measured K_d of 1.1 ± 0.2 μM (data not shown) was very similar to that observed for wild-type SecA, consistent with the normal in vivo function and robust ATPase activities of the SecA monocysteine mutants used in this study. Furthermore, the specificity of the binding interaction was tested by using a scrambled SP22 signal peptide derivative that contained a cysteine residue at position 22 but lacked both the positively charged amino-terminal and hydrophobic core regions. These measurements were also used to ensure that at the experimental concentrations of a nonphysiological ligand and SecA protein there was no significant background FRET in our system. We utilized SecA-Cys-190 for this control experiment because of the high FRET efficiency observed for this pair as described above (Table 1). Under our conditions (7 μM IAEDANS-labeled SecA-Cys-190 and 18 μM IANBD-labeled scrambled SP22), neither high-affinity binding nor FRET was detected (data not shown). These measurements demonstrate that nonspecific binding of the signal peptide to SecA was negligible under these conditions and did not contribute to our FRET measurements.

Representative spectra used for our FRET mapping study are presented (Figure S1 of the Supporting Information), and the distance results are listed in Table 1. FRET efficiencies were calculated on the basis of the quenching of donor emission according to the method described by Lakowicz (*55*, *63*), and distances were measured for 13 SecA-Cys mutants with SP22 and five SecA-Cys mutants with SP2. Since FRET efficiencies have a sixth-order dependence on the distance between the fluorophores, the most reliable distance determinations occur in a FRET efficiency range from 10 to 80% or $0.5R_0$ to $1.5R_0$. In general, the distances measured range from 26 to 59 Å with a relatively small error as determined from multiple measurements. R_0 values were calculated for most donor−acceptor pairs, and they were found to lie in the 30−40 Å range, with an average value of 33.7 Å (Table 1). The variations in R_0 were primarily related to the quantum yield of the donor, which was affected by the placement of the probe on SecA.

The FRET efficiencies measured lie in four distinct classes: highly efficient (≥ 0.7), moderately efficient ($0.3 \leq E < 0.7$), fairly efficient ($0.1 \leq E < 0.3$), and poorly efficient (< 0.1). Many of the efficiencies lie in the moderate to high range, and these distances were most useful for defining the binding site. Nevertheless, the broad range of efficiencies and consequently distances observed suggest that the FRET donor−acceptor pairs sampled a relatively large area of SecA topology for the identification of the signal peptide-binding site. In the case of the SP22 peptide, FRET efficiencies measured with SecA-Cys-190 and SecA-Cys-287 are in the highly efficient range while SecA-Cys-256, SecA-Cys-292, SecA-Cys-371, SecA-Cys-661, and SecA-Cys-718 lie in the moderately efficient range. While most of the mutants in these first two categories have their cysteine residue located within PPXD, the latter two mutants are significant, since these cysteine residues are located within the HSD and HWD, respectively. In addition, Cys-190 lies at the NDB-1, HSD, and PPXD interface, and it is close to the region recently proposed to be a clamp for binding peptide (Figure 1) (*10*). These results are consistent with recent reports that place portions of the SecA signal peptide-binding domain close to the NBD-1, PPXD, and HSD interdomain interface (*25*, *36*, *38*). By contrast, the weakest transfer efficiencies, corresponding to distances of ~50 Å and longer, were observed for mutants located at the NBD-1−NBD-2 interface (SecA-Cys-402) or within NBD-2 itself (SecA-Cys-447, SecA-Cys-470, and SecA-Cys-506), which on the basis of the available literature (reviewed in the introductory section) are remote from the signal peptide-binding site. In addition, these distances were also consistent with measurements from these residues to portions of PPXD utilizing the *B. subtilis* SecA crystal structures (unfortunately, the *E. coli* SecA X-ray structure is missing electron density for most of PPXD) (*3*, *34*, *64*).

FRET efficiencies were measured for SP2 with SecA mutants located within NBD-1, PPXD, and HSD. These measurements are within the moderate range of FRET efficiency and largely confirmed the distances measured for SP22. The differences in transfer efficiencies between SP2 and SP22 for a given SecA mutant are attributed to the different locations of the probe on the peptide (N-terminal vs C-terminal), and the fact that the N-terminal region of the peptide is fairly mobile and flexible as shown by the NMR solution structure of the SecA-bound signal peptide (*38*). This flexibility is also reflected in our anisotropy data for the SecA−signal peptide complex, which indicates that residue 2 of SP2 displayed significantly greater mobility than residue 22 of SP22 [0.26 and 0.13, respectively (Figure 3)].

A number of factors need to be considered in interpreting our data. (i) The point of attachment of the probes to SecA or signal peptide may modestly affect our distance measurements (by up to ~7−10 Å) based on the size of these probes. The dihedral flexibility introduced by the covalent attachment of the dyes to the protein or peptide also contributes to the overall uncertainty in the distance. (ii) The assumption of random orientation of the bound dyes (κ^2 in eq 4 of Experimental Procedures) contributes to the uncertainty in the calculated distances. We note that for a number of labeled SecA mutants investigated, the dyes were relatively mobile as measured by anisotropy, and thus, the assumption of $^2/_3$ for the κ^2 value most likely leads to an error of only ≤10% in the distance measured (*55*). (iii) Since FRET measurements are taken in bulk, they represent an average of all the conformations present in solution. The NMR and multiple X-ray structures of SecA point to a conformationally dynamic protein, where it is estimated that approximately 10% of SecA exists in a closed conformation in solution where PPXD undergoes an ~60° solid body rotation to associate with the HSD and HWD (*38*). Thus, our FRET measurements represent a weighted average of SecA in its open and closed conformational states. The relative population of the closed conformational state is unclear as it depends on the signal peptide binding affinity of SecA in this form. However, we assume that this contribution to our FRET efficiency is no higher than 10%, consistent with the limits of our measured stoichiometry of signal peptide binding to SecA of 1:1. (iv) One or more of the mutant SecA proteins utilized here may be

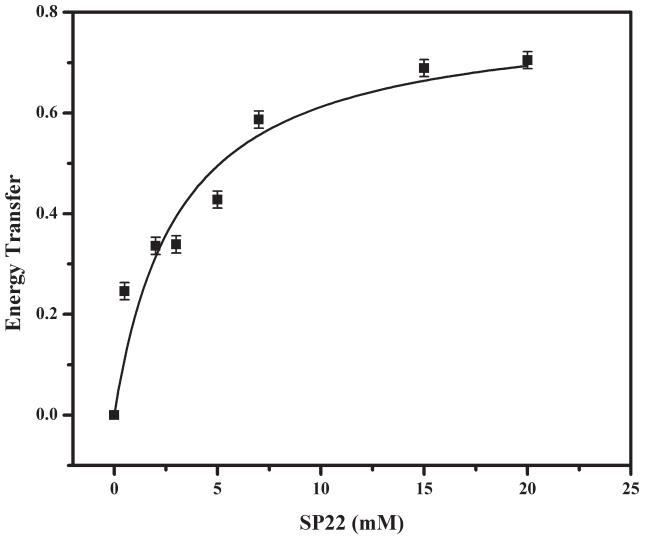

FIGURE 5: Equilibrium binding of SP22 to monomeric SecA. Binding of IANBD-labeled SP22 to IAEDANS-labeled SecAΔ11-Cys-190 (■) was assessed by FRET. SecAΔ11-Cys-190 was maintained at a constant concentration of 0.05 μM, and SP22 was titrated into the system from 0 to 15 μM. All experiments were performed in TKE buffer at 20 °C.

significantly altered in their monomer−dimer equilibrium, and therefore, it may exist in a mixture of the monomer and dimer under our conditions. However, as we indicate above, there is no evidence of a difference in the SecA signal peptide-binding sites between these two forms based on their similar binding affinities (compare Figures 3 and 5).

Mapping of the Signal Peptide-Binding Site on SecA. To visually locate the signal peptide-binding domain on the SecA structure, we mapped the intersection of our FRET distances for SP22 or SP2 onto all of the existing SecA crystal structures (Figure S3 of the Supporting Information) as well as the NMR solution structure of SecA (*38*) (Figure 6A). For this purpose, each experimentally measured distance was entered into Jmol (http://Jmol.sourceforge.net) to create a potential signal peptide-binding spherical surface around any given SecA cysteine residue. This surface was defined as the measured FRET distance with associated error. The overlapping regions were then identified by creation of a Jmol script that highlighted the SecA structural regions shared in common for the entire data set. The SecA signal peptide-binding domain identified in this manner is relatively large and consists of approximately 20% of the total SecA residues. It is generally consistent for all of the different SecA structures that have been determined thus far with some minor variations. Thus, for all of the X-ray structures of SecA, regardless of organism (*3*, *34*, *64*−*66*), the FRET-identified site maps mainly to PPXD (> 50%), but importantly, it includes significant portions of HSD, particularly the two-helix finger subdomain previously implicated in preprotein interaction and translocation (*10*, *11*). The tip of the two-helix finger, where preprotein cross-linking was shown to occur, is not contained in our binding site for all of the SecA X-ray structures. Rather, its inclusion is observed for the *E. coli* SecA X-ray (*3*) and NMR structures (*38*), where the PPXD is observed to be in the orientation associated with the open state of SecA, which has been suggested to be the more physiological state (*38*). The parallel SecA dimer of *Thermus thermophilus* (*66*) contains the smallest amount of our signal peptide-binding surface within HSD. In addition, a few residues from NBD-1 are included in our SecA signal peptide-binding domain for most of these organisms because of its proximity to the PPXD−HSD interdomain interface.

We chose to use the NMR solution structure of *E. coli* SecA for display purposes (*38*), since it is closest to our solution FRET conditions. The majority of the binding site is defined by both SP2- and SP22-determined distances (Figure 6A), largely due to the higher transfer efficiencies observed for the SecA−SP2 donor−acceptor pairs, which causes a high degree of overlap between the two data sets. The binding domain determined by FRET is significantly larger than that identified by previous studies (Figure 6B), although it is in good overall agreement with the different genetic, biochemical, and biophysical approaches that identified this region of SecA (*25*, *36*, *38*). We note that the longest dimension of our binding site is ~40 Å along the long helix of HSD, and this distance compares well with the length of the SecA-bound signal peptide from the NMR study that measured ~46 Å for KRR-LamB residues 1−22 (*38*). The signal peptide length is necessarily determined by the amount of secondary structure present, and currently the NMR solution structure, which includes ~30 Å of unstructured regions of KRR-LamB, represents the best structural model for our study.

Although our FRET-determined signal peptide-binding domain encompasses all of the residues that experienced the greatest chemical shift in the NMR study (*38*), our study identifies a potentially different binding site (Figure 6B). In particular, most of the NMR-determined site is confined to portions of PPXD and includes a thin strip of residues within HSD that align with the strands connecting PPXD to NBD-1 (Figure 6C) (*38*). By contrast, our FRET-determined site includes large portions of the HSD, including the two-helix finger domain that has been shown to interact with preprotein and is inserted into the mouth of the SecYEG channel where it has been proposed to act as a ratchet to drive protein translocation (Figure 6D,E) (*10*, *11*). On the basis of this juxtaposition, we propose a model in which the signal peptide would bind along the axes of the helices of HSD, and the two-helix finger would promote the insertion of the bound signal peptide into the SecYEG channel. This proposal is consistent with our signal peptide-binding site and the geometry of the SecA−SecYEG complex, whereas the location of the bound amino-terminal region of the SecA-bound KRR-LamB signal peptide (i.e., orthogonal rather than parallel to the helices of HSD) would require an additional major conformational change of SecA to move the signal peptide into the mouth of the SecYEG channel. In support of our model, we note that the long helix of HSD has been implicated in driving the chemo-mechanical movement necessary for SecA-dependent protein translocation (*67*). Furthermore, a number of residues within HSD have also been implicated in preprotein interaction according to a recent EPR-based mapping study (*39*). Very recently, a *B. subtilis* SecA crystal structure has been determined with a hydrophilic peptide bound to mimic the preprotein (*40*). In this structure, peptide electron density is observed at the back of the clamp region. This β-sheet region, which connects the PPXD with HSD and NBD-1, is fully contained within the FRET-determined site. This crystallographic finding lends further support to the identification of a physiological binding site for the signal peptide by FRET, which is different in orientation from the NMR-identified site.

Finally, we believe that it is significant that the C-terminal "tail" or CTL domain of SecA occupies our FRET-determined peptide-binding domain (*34*), which is consistent with its peptide-binding nature. In addition, it was recently shown that the

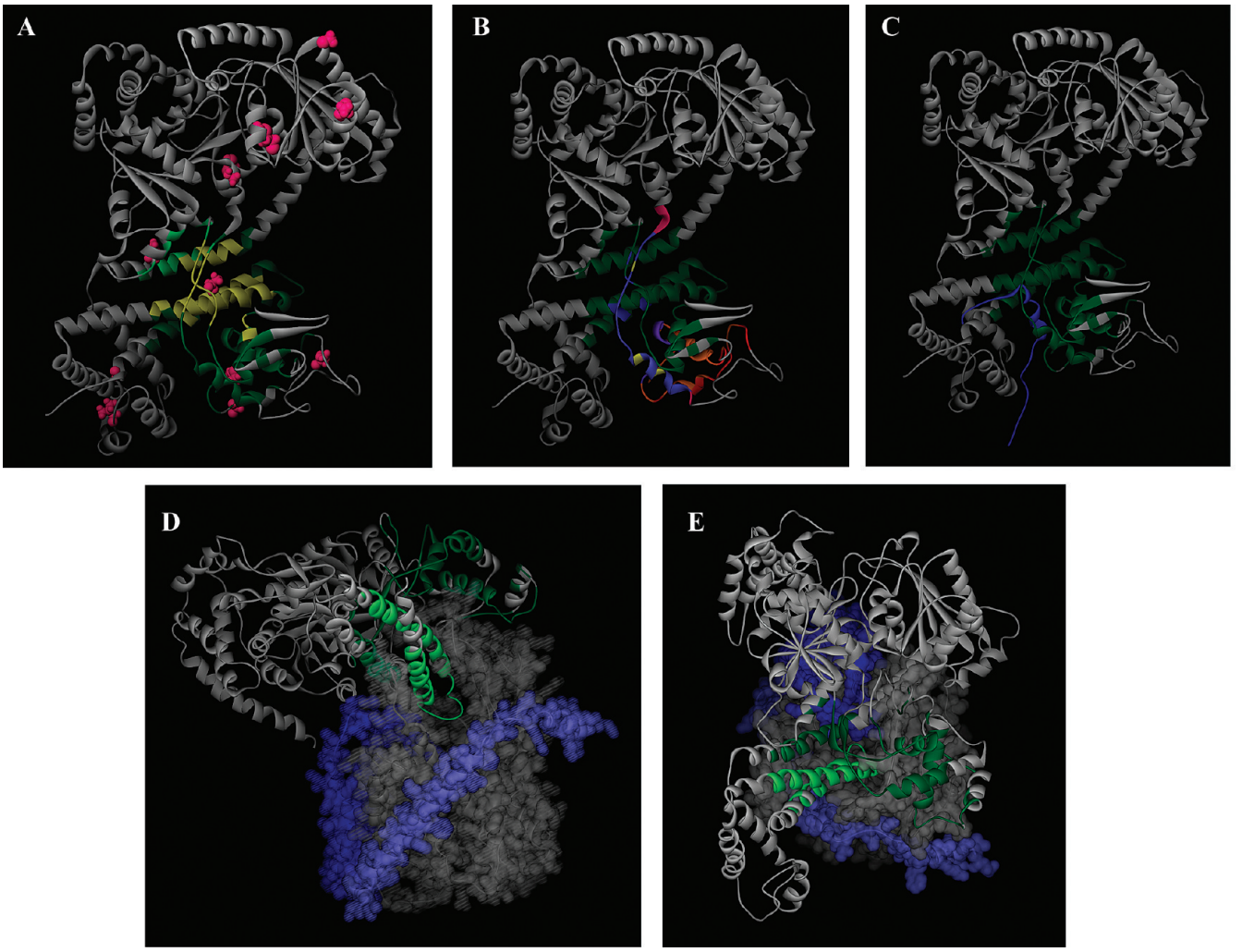

FIGURE 6: Location of the SecA signal peptide-binding domain. (A) A model of the NMR structure of *E. coli* SecA (Protein Data Bank entry 2VDA structure 1) (*38*) is shown in a gray-colored ribbon representation. The SecA region in common for the SP22 and SP2 data sets is colored yellow, while those residues specific for SP22 and SP2 are colored dark and light green, respectively. The cysteine residues utilized for mapping are colored magenta. (B) Similar to panel A except the different SecA signal peptide-binding sites are color-coded for comparison to highlight overlapping and nonoverlapping regions: green, red, and magneta for nonoverlapping regions of our site compared to that determined by Musial-Siwek et al. (*36*) and Baud et al. (*25*), respectively; dark blue, orange, and light blue for single overlapping regions of our site with that determined by Gelis et al., Musial-Siwek et al., and Baud et al., respectively; purple and yellow for double overlapping regions of our site with that determined by both Gelis et al. and Musial-Siwek et al. or both Gelis et al. and Baud et al., respectively. (C) Comparison of the SecA-bound KRR-LamB signal peptide structure (Protein Data Bank entry 2VDA SP structure 1) with our FRET-mapped signal peptide-binding domain, which is colored green. The KRR-LamB signal peptide is colored blue, and its amino terminus is located at the bottom of the figure. (D) A model of the cocrystal structure of the *Thermotoga maritima* SecA−SecYEG complex (Protein Data Bank entry 3din) (*10*) viewed from the side. Most of SecA is shown in a gray-colored ribbon representation, SecY as a gray solid surface structure, SecE as a light blue solid surface structure, and SecG as a dark blue solid surface structure. The FRET-mapped SecA signal peptide-binding domain is colored dark green, except for those regions that fall within the two-helix finger, which are colored light green for the sake of clarity. SecA residues 668−741 are not shown for the sake of clarity of presentation of the two-helix finger. (E) Similar to panel D except viewed from the cytoplasm.

C-terminal tail of SecA serves an autoinhibitory role for signal peptide binding (i.e., presumably by competing with the binding of the signal peptide) (*38*). Our model is also consistent with the location of the unstructured C-terminal region of the bound signal peptide in the NMR study (residues 21−28), which occupies this region (Figure 6C) (*38*). These observations in the context of our study indicate that additional work is clearly needed to further refine the location of the signal peptide-binding domain of SecA and its conformational movements during the translocation cycle as well as its mode of regulation.

At this time, we cannot rule out the possibility that different signal peptides may bind to slightly different regions of SecA, although depending on the proximity of binding sites such a possibility would appear to create mechanistic complications for initiation of the SecA-dependent translocation cycle at the SecYEG channel. The observed differences could arise because the 28-residue KRR-LamB signal peptide utilized in the NMR study (*38*) has an artificially elongated amino-terminal region, where residues 9−28 correspond to residues 2−21, respectively, of our alkaline phosphatase signal peptide. Indeed, Lys-7, Arg-8, Arg-9, and Lys-10 of KRR-LamB were observed to form salt bridges with appropriate acidic residues of SecA, while the region preceding these residues was found to be relatively unstructured and mobile. Thus, this charged region probably influences the stability of the complex as a result of the salt bridges, which enhance the SecA signal peptide interaction (*20*, *27*) as well as the potential structural stability afforded by a more internal location of the positive charge (i.e., comparison of Arg-9 vs Lys-2 of the

two signal peptides). Such increased stability is further indicated by the significantly weaker binding affinity observed for the wild-type LamB signal peptide with SecA (100 μM vs 3 μM for KRR-LamB) (*38*). Thus, the placement of this region in the NMR structure may be strongly influenced by the interactions of these particular residues. In addition, although NMR measurements provide a greater level of structural detail relative to FRET measurements, the high concentrations of protein and ligand that are employed can lead to nonspecific interactions, particularly in this system where both signal peptides and SecA can aggregate or show artificial associations at high concentrations (> 30 μM). By contrast, FRET-based methods can be performed at more biochemically relevant protein and ligand concentrations, although the structural resolution of a binding site can only be achieved by systematically sampling large regions of the protein surface by moving the appropriate probes along the protein from one location to another. Nevertheless, the relative agreement between the results of our two groups is striking, given the fact that different structural methods and signal peptides were utilized in the two studies.

Given the development of a robust fluorescence-based signal peptide binding assay as well as FRET-based mapping in this system, a number of additional studies can now be pursued. These include genetic confirmation and mechanistic exploration of the SecA signal peptide-binding domain as well as mapping of the region of SecA involved in binding of the early mature region of the preprotein, to name just a couple of possibilities. In addition, the fact that the signal peptide-binding domain identified here lies at the center of the SecA molecule and is flanked by domains that interact with ATP and the SecYEG channel component suggests obvious experiments for further exploring the details of the chemo-mechanical cycle of SecA utilizing a multidisciplinary approach to this problem.

ACKNOWLEDGMENT

We thank Dylan Maxwell Reilly for assistance in creating the Jmol script and Lorry Grady and Sanchaita Das for intellectual discussions during the course of the study and feedback on this paper.

SUPPORTING INFORMATION AVAILABLE

Representative result of our FRET study for IAEDANS-labeled SecA-Cys-827 and IANBD-labeled SP22 (Figure S1), binding affinity of unlabeled SP2 and IANBD-labeled SP2 with IAEDANS-labeled SecA-Cys-256 (Figure S2) and mapping of the FRET-determined signal peptide-binding site on the SecA crystal structures of *B. subtilis*, *E. coli*, *T. thermophilus*, and *Mycobacterium tuberculosis* (Figure S3). This material is available free of charge via the Internet at http://pubs.acs.org.

REFERENCES

1. Driessen, A. J., and Nouwen, N. (2008) Protein translocation across the bacterial cytoplasmic membrane. *Annu. Rev. Biochem. 77*, 643–667.
2. Papanikou, E., Karamanou, S., and Economou, A. (2007) Bacterial protein secretion through the translocase nanomachine. *Nat. Rev. Microbiol. 5*, 839–851.
3. Papanikolau, Y., Papadovasilaki, M., Ravelli, R. B., McCarthy, A. A., Cusack, S., Economou, A., and Petratos, K. (2007) Structure of dimeric SecA, the *Escherichia coli* preprotein translocase motor. *J. Mol. Biol. 366*, 1545–1557.
4. Cabelli, R. J., Dolan, K. M., Qian, L. P., and Oliver, D. B. (1991) Characterization of membrane-associated and soluble states of SecA protein from wild-type and SecA51(TS) mutant strains of *Escherichia coli*. *J. Biol. Chem. 266*, 24420–24427.
5. Hartl, F. U., Lecker, S., Schiebel, E., Hendrick, J. P., and Wickner, W. (1990) The binding cascade of SecB to SecA to SecY/E mediates preprotein targeting to the *E. coli* plasma membrane. *Cell 63*, 269–279.
6. Woodbury, R. L., Hardy, S. J., and Randall, L. L. (2002) Complex behavior in solution of homodimeric SecA. *Protein Sci. 11*, 875–882.
7. Rusch, S. L., and Kendall, D. A. (2007) Oligomeric states of the SecA and SecYEG core components of the bacterial Sec translocon. *Biochim. Biophys. Acta 1768*, 5–12.
8. Economou, A., and Wickner, W. (1994) SecA promotes preprotein translocation by undergoing ATP-driven cycles of membrane insertion and deinsertion. *Cell 78*, 835–843.
9. van der Wolk, J. P., de Wit, J. G., and Driessen, A. J. (1997) The catalytic cycle of the *Escherichia coli* SecA ATPase comprise two distinct preprotein translocation events. *EMBO J. 16*, 7297–7304.
10. Zimmer, J., Nam, Y., and Rapoport, T. (2008) Structure of a complex of the ATPase SecA and the protein-translocation channel. *Nature 455*, 936–943.
11. Erlandson, K. J., Miller, S., Nam, Y., Osborne, A. R., Zimmer, J., and Rapoport, T. (2008) A role for the two-helix finger of the SecA ATPase in protein translocation. *Nature 455*, 984–988.
12. Cabelli, R. J., Chen, L., Tai, P. C., and Oliver, D. B. (1988) SecA protein is required for secretory protein translocation into *E. coli* membrane vesicles. *Cell 55*, 683–692.
13. Randall, L. L., and Hardy, S. J. (2002) SecB, one small chaperone in the complex milieu of the cell. *Cell. Mol. Life Sci. 59*, 1617–1623.
14. Karamyshev, A. L., and Johnson, A. E. (2005) Selective SecA association with signal sequences in ribosome-bound nascent chains: A potential role for SecA in ribosome targeting to the bacterial membrane. *J. Biol. Chem. 280*, 37930–37940.
15. Lill, R., Cunningham, K., Brundage, L. A., Ito, K., Oliver, D., and Wickner, W. (1989) SecA protein hydrolyzes ATP and is an essential component of the protein translocation ATPase of *Escherichia coli*. *EMBO J. 8*, 961–966.
16. Cunningham, K., and Wickner, W. (1989) Specific recognition of the leader region of precursor proteins is required for the activation of translocation ATPase of *Escherichia coli*. *Proc. Natl. Acad. Sci. U.S.A. 86*, 8630–8634.
17. Triplett, T. L., Sgrignoli, A. R., Gao, F. B., Yang, Y. B., Tai, P. C., and Gierasch, L. M. (2001) Functional signal peptides bind a soluble N-terminal fragment of SecA and inhibit its ATPase activity. *J. Biol. Chem. 276*, 19648–19655.
18. Lill, R., Dowhan, W., and Wickner, W. (1990) The ATPase of SecA is regulated by acidic phospholipids, SecY, and the leader and mature domains of precursor proteins. *Cell 60*, 271–280.
19. Miller, A., Wang, L., and Kendall, D. A. (1998) Synthetic signal peptides specifically recognize SecA and stimulate ATPase activity in the absence of preprotein. *J. Biol. Chem. 273*, 11409–11412.
20. Wang, L., Miller, A., and Kendall, D. A. (2000) Signal peptide determinants of SecA binding and stimulation of ATPase activity. *J. Biol. Chem. 275*, 10154–10159.
21. Kimura, E., Akita, M., Matsuyama, S., and Mizushima, S. (1991) Determination of a region in SecA that interacts with presecretory proteins in *Escherichia coli*. *J. Biol. Chem. 266*, 6600–6606.
22. Joly, J. C., and Wickner, W. (1993) The SecA and SecY subunits of translocase are the nearest neighbors of a translocating preprotein, shielding it from phospholipids. *EMBO J. 12*, 255–263.
23. Shinkai, A., Mei, L. H., Tokuda, H., and Mizushima, S. (1991) The conformation of SecA, as revealed by its protease sensitivity, is altered upon interaction with ATP, presecretory proteins, everted membrane vesicles, and phospholipids. *J. Biol. Chem. 266*, 5827–5833.
24. Ding, H., Mukerji, I., and Oliver, D. (2001) Lipid and signal peptide-induced conformational changes within the C-domain of *Escherichia coli* SecA protein. *Biochemistry 40*, 1835–1843.
25. Baud, C., Karamanou, S., Sianidis, G., Vrontou, E., Politou, A. S., and Economou, A. (2002) Allosteric communication between signal peptides and the SecA protein DEAD motor ATPase domain. *J. Biol. Chem. 277*, 13724–13731.
26. Musial-Siwek, M., Rusch, S. L., and Kendall, D. A. (2005) Probing the affinity of SecA for signal peptide in different environments. *Biochemistry 44*, 13987–13996.
27. Akita, M., Sasaki, S., Matsuyama, S., and Mizushima, S. (1990) SecA interacts with secretory proteins by recognizing the positive charge at the amino terminus of the signal peptide in *Escherichia coli*. *J. Biol. Chem. 265*, 8164–8169.
28. Mori, H., Araki, M., Hikita, C., Tagaya, M., and Mizushima, S. (1997) The hydrophobic region of signal peptides is involved in the

interaction with membrane-bound SecA. *Biochim. Biophys. Acta 1326*, 23–36.
29. Chou, Y. T., and Gierasch, L. M. (2005) The conformation of a signal peptide bound by *Escherichia coli* preprotein translocase SecA. *J. Biol. Chem. 280*, 32753–32760.
30. Izard, J. W., Rusch, S. L., and Kendall, D. A. (1996) The amino-terminal charge and core region hydrophobicity interdependently contribute to the function of signal sequences. *J. Biol. Chem. 271*, 21579–21582.
31. Bedouelle, H., Bassford, P. J., Jr., Fowler, A. V., Zabin, I., Beckwith, J., and Hofnung, M. (1980) Mutations which alter the function of the signal sequence of the maltose binding protein of *Escherichia coli*. *Nature 285*, 78–81.
32. Goldstein, J., Lehnhardt, S., and Inouye, M. (1991) In vivo effect of asparagine in the hydrophobic region of the signal sequence. *J. Biol. Chem. 266*, 14413–14417.
33. Kendall, D. A., Doud, S. K., and Kaiser, E. T. (1990) A comparative analysis of single- and multiple-residue substitutions in the alkaline phosphatase signal peptide. *Biopolymers 29*, 139–147.
34. Hunt, J. F., Weinkauf, S., Henry, L., Fak, J. J., McNicholas, P., Oliver, D. B., and Deisenhofer, J. (2002) Nucleotide control of interdomain interactions in the conformational reaction cycle of SecA. *Science 297*, 2018–2026.
35. Papanikou, E., Karamanou, S., Baud, C., Frank, M., Sianidis, G., Keramisanou, D., Kalodimos, C. G., Kuhn, A., and Economou, A. (2005) Identification of the preprotein binding domain of SecA. *J. Biol. Chem. 280*, 43209–43217.
36. Musial-Siwek, M., Rusch, S. L., and Kendall, D. A. (2007) Selective photoaffinity labeling identifies the signal peptide binding domain on SecA. *J. Mol. Biol. 365*, 637–648.
37. Kourtz, L., and Oliver, D. (2000) Tyr-326 plays a critical role in controlling SecA-preprotein interaction. *Mol. Microbiol. 37*, 1342–1356.
38. Gelis, I., Bonvin, A. M., Keramisanou, D., Koukaki, M., Gouridis, G., Karamanou, S., Economou, A., and Kalodimos, C. G. (2007) Structural basis for signal-sequence recognition by the translocase motor SecA as determined by NMR. *Cell 131*, 756–769.
39. Cooper, D. B., Smith, V. F., Crane, J. M., Roth, H. C., Lilly, A. A., and Randall, L. L. (2008) SecA, the motor of the secretion machine, binds diverse partners on one interactive surface. *J. Mol. Biol. 382*, 74–87.
40. Zimmer, J., and Rapoport, T. A. (2009) Conformational Flexibility of the ATPase SecA Enables Peptide Interaction and Translocation. *J. Mol. Biol. 394*, 606–612.
41. Lorenz, M., and Diekmann, S. (2006) Distance determination in protein-DNA complexes using fluorescence resonance energy transfer. *Methods Mol. Biol. 335*, 243–255.
42. Lohse, M. J., Hoffmann, C., Nikolaev, V. O., Vilardaga, J. P., and Bunemann, M. (2007) Kinetic analysis of G protein-coupled receptor signaling using fluorescence resonance energy transfer in living cells. *Adv. Protein Chem. 74*, 167–188.
43. Piston, D. W., and Kremers, G. J. (2007) Fluorescent protein FRET: The good, the bad and the ugly. *Trends Biochem. Sci. 32*, 407–414.
44. Edidin, M. (2003) Fluorescence resonance energy transfer: Techniques for measuring molecular conformation and molecular proximity. Current Protocols in Immunology, Chapter 18, Unit 18.10, Wiley, New York.
45. Heyduk, T. (2002) Measuring protein conformational changes by FRET/LRET. *Curr. Opin. Biotechnol. 13*, 292–296.
46. Natale, P., den Blaauwen, T., van der Does, C., and Driessen, A. J. (2005) Conformational state of the SecYEG-bound SecA probed by single tryptophan fluorescence spectroscopy. *Biochemistry 44*, 6424–6432.
47. Ding, H., Mukerji, I., and Oliver, D. (2003) Nucleotide and phospholipid-dependent control of PPXD and C-domain association for SecA ATPase. *Biochemistry 42*, 13468–13475.
48. Ding, H., Hunt, J. F., Mukerji, I., and Oliver, D. (2003) *Bacillus subtilis* SecA ATPase exists as an antiparallel dimer in solution. *Biochemistry 42*, 8729–8738.
49. Or, E., Navon, A., and Rapoport, T. (2002) Dissociation of the dimeric SecA ATPase during protein translocation across the bacterial membrane. *EMBO J. 21*, 4470–4479.
50. Studier, F. W., Rosenberg, A. H., Dunn, J. J., and Dubendorff, J. W. (1990) Use of T7 RNA polymerase to direct expression of cloned genes. *Methods Enzymol. 185*, 60–89.
51. Jilaveanu, L. B., and Oliver, D. (2007) In vivo membrane topology of *Escherichia coli* SecA ATPase reveals extensive periplasmic exposure of multiple functionally important domains clustering on one face of SecA. *J. Biol. Chem. 282*, 4661–4668.
52. Jilaveanu, L. B., Zito, C. R., and Oliver, D. (2005) Dimeric SecA is essential for protein translocation. *Proc. Natl. Acad. Sci. U.S.A. 102*, 7511–7516.
53. Lanzetta, P. A., Alvarez, L. J., Reinach, P. S., and Candia, O. A. (1979) An improved assay for nanomole amounts of inorganic phosphate. *Anal. Biochem. 100*, 95–97.
54. Mitchell, C., and Oliver, D. (1993) Two distinct ATP-binding domains are needed to promote protein export by *Escherichia coli* SecA ATPase. *Mol. Microbiol. 10*, 483–497.
55. Lakowicz, J. R. (1999) Principles of fluorescence spectroscopy, 2nd ed., Plenum Publishers, New York.
56. Crosby, G. A., and Demas, J. N. (1971) The Measurement of photoluminescence quantum yields. A review. *J. Phys. Chem. 75*, 991–1024.
57. Izard, J. W., Doughty, M. B., and Kendall, D. A. (1995) Physical and conformational properties of synthetic idealized signal sequences parallel their biological function. *Biochemistry 34*, 9904–9912.
58. Alvear, M., Encinas, M. V., Herrera, L., and Cardemil, E. (1994) Resonance Energy transfer determination of the distance between the four cysteine-364 residues in *Saccharomyces cerevisiae* phosphoenolpyruvate carboxylkinase. *Arch. Biochem. Biophys. 309*, 231–238.
59. Haache, A., Broadley, S. A., Boteva, R., Tzvetkov, N., Hartl, F. U., and Breuer, P. (2006) Proteolytic cleavage of polyglutamine-expanded ataxin-3 is critical for aggregation and sequestration of non-expanded ataxin-3. *Hum. Mol. Genet. 15*, 555–568.
60. Lill, R., Cunningham, K., Brundage, L. A., Ito, K., Oliver, D., and Wickner, W. (1989) SecA protein hydrolyzes ATP and is an essential component of the protein translocation ATPase of *Escherichia coli*. *EMBO J. 8*, 961–966.
61. Das, S., Stivison, E., Folta-Stogniew, E., and Oliver, D. (2008) Reexamination of the role of the amino terminus of SecA in promoting its dimerization and functional state. *J. Bacteriol. 190*, 7302–7307.
62. Benach, J., Chou, Y. T., Fak, J. J., Itkin, A., Nicolae, D. D., Smith, P. C., Wittrock, G., Floyd, D. L., Golsaz, C. M., Gierasch, L. M., and Hunt, J. F. (2003) Phospholipid-induced monomerization and signal-peptide-induced oligomerization of SecA. *J. Biol. Chem. 278*, 3628–3638.
63. Clegg, R. M. (1992) Fluorescence resonance energy transfer and nucleic acids. *Methods Enzymol. 211*, 353–388.
64. Zimmer, J., Li, W., and Rapoport, T. A. (2006) A novel dimer interface and conformational changes revealed by an X-ray structure of *B. subtilis* SecA. *J. Mol. Biol. 364*, 259–265.
65. Sharma, V., Arockiasamy, A., Ronning, D. R., Savva, C. G., Holzenburg, A., Braunstein, M., Jacobs, W. R., Jr., and Sacchettini, J. C. (2003) Crystal structure of *Mycobacterium tuberculosis* SecA, a preprotein translocating ATPase. *Proc. Natl. Acad. Sci. U.S.A. 100*, 2243–2248.
66. Vassylyev, D. G., Mori, H., Vassylyeva, M. N., Tsukazaki, T., Kimura, Y., Tahirov, T. H., and Ito, K. (2006) Crystal structure of the translocation ATPase SecA from *Thermus thermophilus* reveals a parallel, head-to-head dimer. *J. Mol. Biol. 364*, 248–258.
67. Mori, H., and Ito, K. (2006) The long α-helix of SecA is important for the ATPase coupling of translocation. *J. Biol. Chem. 281*, 36249–36256.